MECHANICAL PERFORMANCE OF 3D-PRINTED CONCRETE CONTAINING NANO CLAYS AND RECYCLED CONCRETE FINES

MAHMUT KEREM SARIKAYA

ÖZYEĞİN UNIVERSITY

AUGUST, 2025

MECHANICAL PERFORMANCE OF 3D-PRINTED CONCRETE CONTAINING NANO CLAYS AND RECYCLED CONCRETE FINES

by
Mahmut Kerem Sarıkaya

Thesis
Submitted in Partial Fulfillment of the
Requirements for the Degree of

Master of Science

in
Civil Engineering

Advisor: Assoc. Prof. Zeynep Başaran Bundur

Graduate School of Science and Engineering
Özyeğin University
İstanbul

August, 2025

MECHANICAL PERFORMANCE OF 3D-PRINTED CONCRETE CONTAINING NANO CLAYS AND RECYCLED CONCRETE FINES

Approved by:

Assoc. Prof. Zeynep Başaran Bundur
Advisor
Department of Civil Engineering
Özyeğin University

Assoc. Prof. Bülent Erkmen
Department of Civil Engineering
Özyeğin University

Assoc. Prof. Çağla Meral Akgül
Department of Civil Engineering
Middle East Technical University

Approval Date: August 5, 2025

To my father, Mehmet İsmail Sarıkaya

DECLARATION OF ORIGINALITY

I hereby declare that I am the sole author of this thesis and that this is the true copy of my thesis, including the final revisions, approved by my thesis committee. All data and information have been obtained, produced, and presented in accordance with the rules of research ethics and principles of academic honesty. As required by these rules, to the best of my knowledge I have acknowledged ideas, thoughts, and any copyrighted material in accordance with the standard referencing rules. I certify that any part of this thesis has not been submitted for a degree or diploma in another educational institution.

Mahmut Kerem Sarıkaya

ABSTRACT

The integration of digital manufacturing technologies into the construction industry has led to a paradigm shift in conventional building practices by enhancing design flexibility, reducing material consumption, and improving overall efficiency. Among these technologies, 3D Concrete Printing (3DCP) offers significant potential by eliminating the need for formwork and enabling layer-by-layer fabrication. However, the mechanical behaviour of 3D-printed elements, particularly concerning interlayer bonding, anisotropy, and lack of reinforcement, differs considerably from traditionally cast concrete, posing challenges for structural reliability.

A comprehensive experimental program was conducted to assess the influence of these additives on the flexural and compressive strength of the printed elements. Additionally, the mechanical properties of 3D-printed specimens were compared with those of conventionally cast counterparts to evaluate the effects of layer orientation and printing-induced anisotropy. A novel shear strength test procedure was developed to characterize the interfacial bonding performance of layered mortar samples.

Furthermore, a numerical simulation of an unreinforced 3D-printed wall element was performed using finite element analysis to predict its lateral load bearing capacity and crack propagation under seismic loading conditions. The study higlights that while nano clay improves buildability, the inclusion of RCF affects compressive strength due to weak interfacial bonding and increased porosity. The findings contribute valuable insights into the design of printable, eco-friendly cementitious composites and underline the need for performance-based evaluation methodologies for 3D-printed structures.

Keywords: 3D-printing, Cement-based materials, Strength, Nano-clay, Recycled concrete fine

ÖZET

Dijital imalat teknolojilerinin inşaat sektörüne entegrasyonu, tasarım esnekliğini artırarak, malzeme tüketimini azaltarak ve genel verimliliğini iyileştirerek geleneksel yapı uygulamalarında önemli bir yenilik getirmiştir. Bu teknolojiler arasında 3B beton baskı, kalıp ihtiyacını ortadan kaldırması ve katman katman üretimi mümkün kılması ile önemli bir potansiyele sahiptir. Ancak özellikle katmanlar arası bağ dayanımı, anizotropi ve donatı eksikliği açısından 3B baskılı elemanların mekanik davranışı, geleneksel olarak uygulanan betonun davranışından önemli ölçüde farklıdır. Bu durum yapısal güvenirlik açısından sorun teşkil etmektedir.

Katkı maddelerinin baskılı elemanların eğilme ve basınç dayanımı üzerine etkisi değerlendirilmiştir. Bunun yanı sıra, katmanlı baskının ve anizotropinin etkisinin değerlendirilmesi için 3B baskılı numunelerin mekanik dayanımı, geleneksel olarak dökülen numuneler ile karşılaştırılmıştır. 3B baskı ile elde edilen katmanlı yapının, yüzey yapışma performansını belirlemek amacıyla kesme dayanımı test prosedürü geliştirilmiştir.

Ayrıca, sismik yükler altında donatısız 3B baskılı bir duvar elemanın yatay yük taşıma kapasitesi ile çatlak ilerlemesinin tahmin edilmesi için sonlu elemanlar analizi kullanılarak sayısal bir simülasyon gerçekleştirilmiştir. Elde edilen sonuçlarda, nano kil inşa edilebilirliği arttırırken, RCF ilavesinin katmanlar arası bağı zayıflattığı ve artan gözeneklilik nedeniyle basınç dayanımını düşürdüğü gözlemlenmiştir. Bu çalışma, yazırılabilir ve çevre dostu çimento esaslı malzemelerin tasarımına katkı sağlamakta ve 3B baskılı yapıların performansa dayalı değerlendirilmesi için yöntemler sunmaktadır.

Anahtar Kelimeler: 3D baskı, Çimento esaslı malzemeler, Mukavemet, Nano kil, Geri dönüştürülmüş beton tozu

ACKNOWLEDGEMENTS

First and foremost, I would like to express my sincere gratitude to Assoc. Prof. Zeynep Başaran Bundur for her invaluable guidance, continuous support, and insightful feedback throughout the course of this research. Her expertise and encouragement played a vital role in shaping the direction and depth of this thesis.

I would also like to extend my heartfelt thanks to Assoc. Prof. Bülent Erkmen, Asst. Prof. Taner Yılmaz and Assoc. Prof. Çağla Meral Akgül for their academic support, critical evaluations, and constructive comments that enriched the quality of my work.

Special thanks go to Ilgın Sandalcı and Tolga Aydın, whose dedication and hard work throughout the semester contributed immensely to the progress and execution of this study.

I am also grateful to my friends and colleagues Mustafa Can Alp, Sami Berat Tever, and Shaghayegh Sadeghzadeh Benam for their constant companionship, motivation, and moral support during both the challenges and successes of this journey.

Lastly, I would like to thank Tolga Törün and Yılmaz Tahtalı for their valuable assistance in the laboratory work, which was essential for the experimental part of this thesis.

This thesis would not have been possible without the support and contributions of all the individuals mentioned above, and I am deeply thankful for their presence throughout this academic endeavor.

TABLE OF CONTENTS

LIST OF TABLES

LIST OF FIGURES

LIST OF ACRONYMS AND ABBREVIATIONS

NM	Nanomontmorillonite
VMA	Viscosity-Modified Agent
RCF	Recycled Concrete Fine
SCMs	Supplementary Cementitious Materials
ASTM	American Society for Testing and Materials
FA	Fly Ash
BFS	Blast Furnace Slag
CSA	Calcium Sulfoaluminate
3DCP	3D Concrete Printing

1. INTRODUCTION

In recent years, digital manufacturing has been identified as the driving force behind the fourth industrial revolution, commonly referred to as Industry 4.0 [1, 2]. The integration of digital manufacturing technologies within the construction sector is transforming traditional practices by enabling the realization of freeform architectural designs, minimizing raw material usage, lowering construction expenditures, and enhancing worker safety [3]. Consequently, over the past decade, digital methods for processing mortar and concrete have garnered considerable attention as alternatives to conventional concrete pumping techniques [4, 5, 6]. Industry analyses suggest that the adoption of digital production methods will imminently reshape the construction industry [7]. Organizations and governmental bodies that proactively adapt to this transformation are likely to secure a competitive advantage within the sector [8].These advancements, however, present a complex challenge for the concrete industry, which must now balance performance enhancement, economic efficiency, and environmental sustainability. Despite ongoing progress, the development of printable construction materials, particularly cement-based formulations, remains a significant technical hurdle [9, 10]. The primary limitation lies in the absence of standardized guidelines or specifications governing material composition for 3D printing applications [11]. As a result, current research efforts are largely centered on establishing standardized practices for digital construction technologies. A key obstacle in this domain is the design of cementitious materials exhibiting high thixotropic behavior, alongside the development of printing equipment capable of ensuring uniform material flow [12]. From a material perspective, printable mortars must demonstrate sufficient workability to facilitate extrusion, while also possessing adequate shape retention post-extrusion to ensure structural integrity (i.e., buildability) [6]. In particular, extrudability and buildability are often conflicting requirements. Enhanced workability promotes extrudability, whereas reduced workability favors buildability. To enable effective layer deposition, it is essential that mortar consistency increases rapidly following extrusion. This behavior is facilitated by the thixotropic properties of cement paste, which allow for swift viscosity changes [13]. However, in systems exhibiting high thixotropy, this rapid viscosity change can result in weak interlayer bonding, as manifested through the formation of cold joints. Consequently, accurately defining the workability window of cementitious materials is of critical importance for ensuring structural performance in digitally fabricated concrete systems.

Despite its growing use, the structural reliability of 3D-printed elements under lateral and seismic loading remains a major research gap. While several studies have investigated the fresh and hardened properties of printable cement-based materials, limited research has focused on their structural performance. This gap is largely due to the lack of design standards and proper characterization of 3D-printed structures. In addition, the layered construction process, anisotropic material behavior, weak interlayer bonding, and lack of conventional reinforcement result in a different structural response from that of traditionally cast concrete [52] .

Understanding the seismic behavior of 3D-printed elements is essential for the broader adoption of this technology in seismically active regions. Current experimental studies and numerical models remain limited in capturing the effects of key parameters such as layer orientation, interfacial bond strength, and geometric irregularities on the lateral load response of 3D-printed concrete [47]. This highlights the growing need for research that integrates material characterization with structural analysis to assess the lateral load-bearing capacity. To date, a comprehensive comparison between cast and 3D-printed samples in terms of material performance remains largely unexplored. A series of experimental and printing procedures were conducted to evaluate the performance of the mix design, followed by structural simulations performed using SAP2000. Afterwards, printed and casted samples were compared in terms of mechanical properties.

In the latest research, additive minerals such as clay have been widely used as rheological modifiers due to their inherent shear-thinning behavior, which stems from their anisotropic surface charges [14]. These opposing charges promote a reversible microstructure that recovers under static conditions and disintegrates when subjected to shear stress [14]. Nano clays can enhance the packing density of cementitious materials by occupying the interstitial spaces between cement particles, thereby strengthening Van der Waals interactions. This improved particle interaction contributes to an increase in thixotropic behavior within cement-based systems [15]. Even though suitable mix designs have been formulated by using various admixtures, additive minerals, or biological applications, the majority of 3D concrete printing applications have remained at the laboratory scale, primarily due to the high cost associated with robotic systems.

1.1 Goal and Objectives

This study aims to investigaye the mechanical performance and interlayer behaviour of 3D-printed cement-based mortars incorporating nano clays and recycled concrete fines /acRCF. The outputs of this study will enhance parameters of 3D printable concrete in terms of sustainability, printability, and structural integrity in digitally fabricated concrete elements. The specific research objectives of the study are as follows:

- To design and optimize printable mortar mixtures using nano clays and RCF to achieve suitable properties for 3D printing.
- To experimentally evaluate the mechanical properties (compressive, flexural and interfacial strength) of 3D-printed specimens in comparison to conventionally cast counterparts.
- To examine the influence of layer orientation and printing parameters on mechanical anisotropy and failure behavior in printed mortar elements.

- To develop a novel test setup for assessing interlayer shear strength in 3D-printed elements and quantify the effects of additive content on bond performance.
- To simulate the structural response of a representative 3D-printed wall under lateral loading using finite element analysis, validating experimental findings at the component scale.

1.2 Outline of the Thesis

This thesis is organized into five chapters, each addressing a critical aspect of the research:

- **Chapter 1.**Provides an introduction to the research topic, outlining the background, motivation, objectives, and scope of the study.
- **Chapter 2.** Presents a comprehensive literature review, highlighting prior investigations on cement-based printable materials and structural simulations, including evaluations by other researchers and previously tested mixture compositions.
- **Chapter 3.** Details the materials and methodologies employed in the study, including the mixing procedures, formulation of the mixtures, and experimental techniques used for characterization.
- **Chapter 4.** Discusses the experimental results and interprets their implications.
- **Chapter 5.** Summarizes the main findings of the research, drawing conclusions and suggesting potential directions for future work.

2. LITERATURE REVIEW

The global population is currently growing at an estimated rate of 1% annually and is expected to reach 9.8 billion by 2050 [16]. The growing population continues to drive increased demand for residential construction, along with other critical infrastructure developments. Concrete is one of the most widely used materials in the world, second only to water in terms of global consumption [17]. However, concrete production consumes substantial quantities of natural resources and accounts for approximately 8% of global anthropogenic CO_2 emissions [18, 19]. Moreover, increasing urbanization leads to higher energy consumption, which negatively impacts the environment [20, 21]. In this context, the identification of sustainable construction materials and the development of appropriate construction techniques have become central concerns for both the construction industry and the academic community. In the pursuit of sustainable construction materials, numerous studies have investigated the use of supplementary cementitious materials (SCMs) as alternatives to cement [22, 23]. These materials can be listed as fly ash [24], silica fume [25], ground granulated blast furnace slag [26] and zeolite [27]. On the other hand, in terms of construction techniques, a novel and innovative technological advancement known as 3D concrete printing has garnered significant global attention due to its potential to revolutionize the construction industry [28, 29]. 3D concrete printing involves the layer-by-layer deposition of concrete using a mobile printing system, eliminating the need for conventional formwork by employing principles of additive manufacturing and robotic engineering [30, 31]. 3D concrete printing presents several advantages over conventional construction methods, including enhanced safety through the reduction of on-site accidents, accelerated construction timelines, mitigation of labor shortages, and a significant reduction in construction waste [30, 32]. Consequently, there is a growing transition toward construction practices that prioritize safety, efficiency, and environmental sustainability, embodying the future direction of digitalized construction.

To this end, the primary focus is on integrating environmentally friendly mix designs with three-dimensional concrete printing applications.

2.1 Sustainable mix designs for 3D-printed concrete

Several studies have conducted extensive experimental investigations to develop sustainable mix designs and adapt them for use in 3D concrete printing. Nikravan et al. [6] reported that the incorporation of clays such as nano montmorillonite and sepiolite, along with the addition of bacteria including Sporosarcina pasteurii and Bacillus megaterium, positively influenced the mechanical properties of 3D-printed mortar. However, their inherent thixotropic characteristics contributed to a reduction in workability. Benam et al. [4] investigated the feasibility of adapting high volume fly ash mortar for 3D printing by modifying its rheological properties through the use of mineral additives. Their findings indicated that the rheology of HVFA mixtures could be enhanced using lime and sepiolite, and that a quaternary mix design offers a promising sustainable alternative for 3D-printed building materials. Kaya et al. [33] expressed that the partial replacement of cement with Fly Ash (FA) and Blast Furnace Slag (BFS) has been shown to significantly reduce carbon emissions and embodied energy, making it an effective strategy for promoting sustainable construction practices. Moreover, among the two, slag demonstrated superior performance in enhancing the buildability and early age structural properties of 3D-printable concrete compared to fly ash. Chen et al. [34] concluded that incorporation of bentonite regulated the rheological properties, including thixotropy and creep, of 3D-printed Calcium Sulfoaluminate (CSA) cement composites. This was achieved through a shear rate and shear stress-controlled protocol designed to ensure the formation of a stable 3D-printed structure. Jin et al. [35] observed that nanomaterials improve the printability and mechanical properties of cementitious mixtures by influencing water absorption, forming a 3D skeleton with cement particles, and accelerating hydration. They also enhance interlayer bonding in 3D-printed structures through moisture retention, filler effects, crack bridging, and hydrate modification. Panda et al. [15] examined how adding nano-clay (NC) affects the fresh properties, mechanical performance, and microstructure of high-volume fly ash (HVFA) mixes for 3D printing. The results revealed that NC significantly enhances thixotropy, improving the mix's suitability for 3D concrete printing. Zeng et al. [36] presents an in-depth experimental study on the triaxial compressive behavior of 3D-printed ultra-high performance concrete reinforced with PE fibers and the results revealed that cubes under triaxial compression showed either column-type or diagonal shear failure. Diagonal shear cracks consistently formed in the YZ plane (perpendicular to the printing direction) when the axial load was applied along the Y or Z directions. Liu et al. [37] explored how the incorporation of recycled rubber aggregates impacts 3D printed concrete and the results showed that the incorporation of recycled rubber aggregates into 3D-printed concrete initially enhances mechanical properties, including compressive and flexural strength, at lower dosages. However, at higher dosages, these strengths decrease due to the inherent material characteristics of rubber, such as low stiffness and weak bonding with the cement matrix.

2.2 The mechanical behaviour of 3D-printed concrete

The mechanical performance of 3D-printed concrete (3DPC) in the hardened state is also critical to the structural integrity and durability of printed elements (Cai et al. [38]). Among the various mechanical properties, shear strength plays a fundamental role in governing failure mechanisms, particularly in regions of stress concentration, load transfer, and interlayer bonding. In 3DCP, where structures are constructed without formwork and through a layer-by-layer deposition process, the hardened shear strength becomes a primary determinant of load-bearing capacity and long-term stability.

In traditional cast concrete, shear forces are primarily resisted through monolithic material behavior. In contrast, 3D printed concrete is inherently anisotropic, due to the directional nature of the printing process. This results in potential weak planes between layers, making the material more susceptible to shear-failure, particularly along interfacial regions. The interlayer performance of 3D printed concrete elements is affected by its composition and printing parameters [38]. Due to the inherent anisotropy and layer-wise construction of 3DPC, shear strength of the concrete is different along different testing directions. To study shear strength of 3DPC along different planes including plane between sequential printing layers, a test method based on that used by Chandrashekharamurthy et al.[39] is developed. The test specimen dimensions are modified to ensure that shear failure occurs along the desired plane before any other failure mode. In addition, the metal formwork can be easily used to have the test specimens with shear plane vertical or parallel to interlayer plane, which enables testing the specimen in different direction.

Shear strength is one of the critical mechanical properties of concrete that affects structural ability to resist loads such as lateral loads, seismic loads, and concentrated loads. Accurate measurement or prediction of shear strength is essential for ensuring safety, stability, and durability of concrete elements such as beams, slabs, and columns since shear failure is often very brittle, sudden and typically catastrophic with little to no warning compared to flexural failure. Therefore, shear failure should be prevented, and it is not a desired mode of failure for structural elements. Accurate measurement of shear strength is vital for ensuring structural integrity, optimizing material use, and complying with the design codes. However, measuring concrete shear strength is complex due to its heterogeneous nature, influence of multiple parameters, loading type and conditions, variability in testing methods and associated technical challenges. The shear failure is rarely isolated. In other words, it often interacts with other failure modes such as flexure or compression, complicating experimental isolation. Failure to measure shear strength accurately can lead to over- or under-designed structures, compromising safety or increasing costs unnecessarily. Common tests, such as the direct shear test, push-off test, or beam shear test, produce different results due to differences in specimen geometry, loading conditions, and boundary effects. For instance, the direct shear test may overestimate strength due to frictional effects at the shear plane [40]. The shear strength of concrete is influenced by the size of the tested specimen. Larger specimens tend to exhibit lower shear strength due to the increased likelihood of defects, as described by the size effect theory [41].

The shear strength of plain and reinforced concrete has been studied by a number of researchers including Hofbeck et al. [40],Sonnenberg et al. [42] using direct shear test on cubic concrete specimens with shear box, Hamadi et al. [43] studied plain web reinforced concrete shear resistance using push-off tests, Mansur et al. [44] investigated shear behavior across a crack by conducting tests on pre-cracked push-off specimens.

One of the commonly used test specimens, which is called push-off specimen, to measure direct shear is shown in Figure 2.1. The specimen rational distribution of stresses has been verified by a number of researchers [45, 46, 47, 48] .However, this specimen geometry is complex, which makes it difficult to cast, and includes reinforcement as shown in Figure 2.1.

Figure 2.1: Direct shear specimen dimension and reinforcement

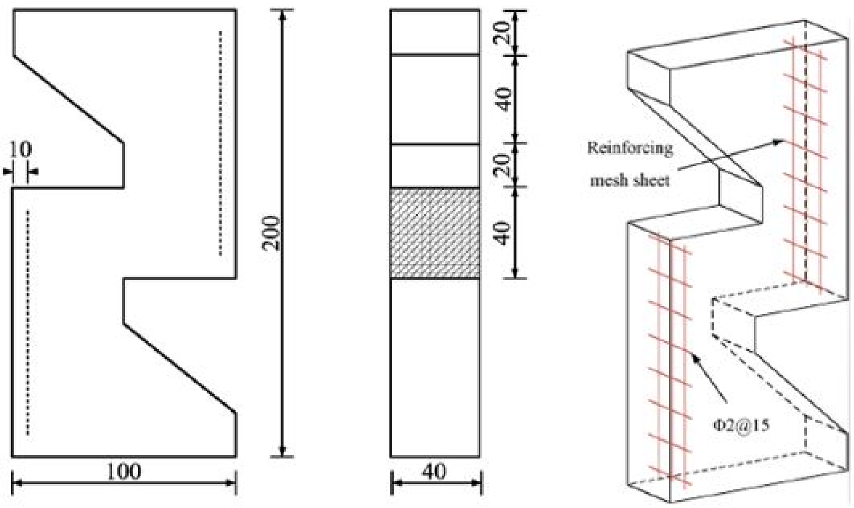

Chandrashekharamurthy et al.[39] used a relatively simple push-off test specimen, as shown in Figure 2.2, as a part of experimental work to determine shear strength of plain concrete and steel fiber reinforced concrete. The specimen is 230 mmx150 mm x150 mm in size. The pre-existing two cracks with 5m opening are to ensure the share failure occurs along the 100 mm long section of the specimen. The specimen is simple to prepare and requires a relatively simple formwork to cast the concrete.

Figure 2.2: Push-off test specimen dimensions and testing

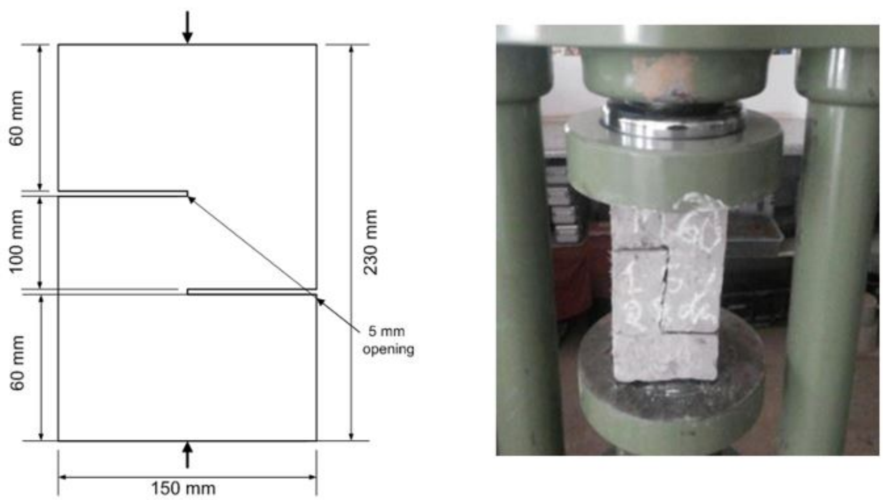

2.3 Contribution of this thesis

This thesis presents a comprehensive investigation into the mechanical performance of 3D-printed cementitious mortars enhanced with Nano Clays and Recycled Concrete Fine (RCF), contributing to both the scientific understanding and practical application of sustainable materials in additive manufacturing for construction. The unique contributions and novelties of this study are as follows:

- **Integration of nano clays and RCF in 3D printable mortars**

  The study explores the combined use of Nano Clays, known for their rheological modification capabilities, and RCF, a waste-derived filler material, within 3D printable mortar systems. This dual approach addresses both the printability-performance trade-off and the valorization of construction waste, which has been scarcely addressed in existing literature.

- **Experimental evaluation of layer-dependent mechanical anisotropy**

  A detailed comparison of mechanical properties between 3D-printed and conventionally cast specimens was conducted, highlighting the anisotropic behavior induced by the layer-by-layer fabrication process. The thesis provides empirical data on the impact of additive content on interlayer bonding strength, compressive strength, and flexural performance.

- **Development of a novel shear bond test for printed interfaces**

  A custom-designed shear strength test procedure was introduced to quantitatively assess the bonding performance at interfacial zones between printed layers. This method offers a reproducible framework for evaluating print-induced weaknesses, which is critical for performance-based validation of 3D-printed concrete structures.

- **Finite element simulation of unreinforced 3D-Printed wall behavior**

  The thesis incorporates a numerical simulation to model the lateral load-bearing behavior and crack patterns of an unreinforced 3D-printed wall element under seismic conditions. This bridges the gap between material-level findings and structural-scale performance predictions, contributing to the digital twin modeling of 3D-printed concrete systems.

- **Sustainability-oriented material design**

  By demonstrating the feasibility of using RCF as a partial cement replacement in printable mortars and optimizing material formulations for reduced environmental impact, the study aligns with global efforts toward circular economy practices and low-carbon construction materials.

3. MATERIALS AND METHODS

3.1 Materials

In this study, the distinct mix designs previously tested for 3D-printability were evaluated in terms of their mechanical behavior [5, 6]. The 3D-printable cement-based mortars were prepared using CEM I type cement. Additionally, different additives were used, including Nanomontmorillonite (NM) as a Viscosity-Modified Agent (VMA),RCF, and fly ash as a Supplementary Cementitious Materials (SCMs).

RCF is concrete waste with a particle size smaller than 4 mm. RCF consists of fine sand and cement paste. It is common to reuse concrete waste with a particle size larger than 4 mm as recycled aggregate in concrete production. Recent studies have demonstrated that the use of RCF in limited replacement ratios has significant potential to reduce carbon emissions and promote the circular economy in the cement industry, particularly when it is carbonated [49].

NM is obtained from Sigma-Aldrich [5]. The particle size of NM is approximately 20 µm. Due to its layered structure, NM exhibits a higher water absorption capacity. It absorbs part of the mixing water, which consequently increases the friction between solid particles [50]. Therefore, the addition of clay improves the rheological properties of cement-based materials. In addition, the particle size of NM is smaller than that of cement, which can lead to a filler effect and provide an additional nucleation site for cement hydration.

The particle size distribution of fine materials was determined using a Mastersizer 2000 particle analyzer equipped with a Hydro MU 2000 wet dispersion unit (Malvern, Worcestershire, United Kingdom). To prevent further hydration of the cement particles, ethanol was used as the dispersion medium. Figure 3.1 presents the particle size distribution of CEM I cement, F-type fly ash, and recycled concrete fines.

Figure 3.1: Particle size distribution

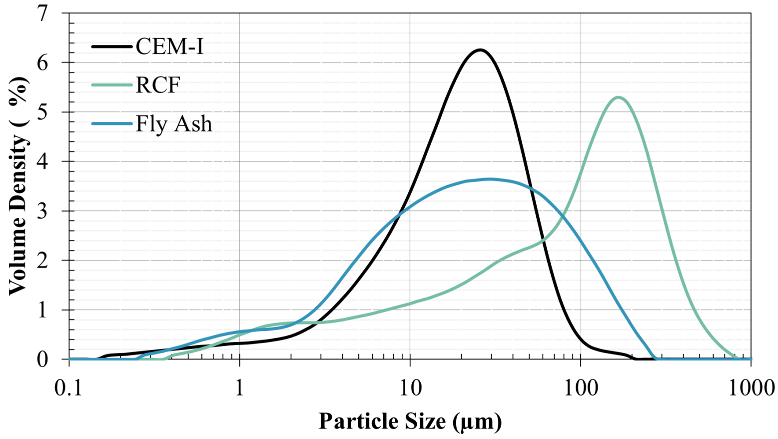

In this study, three types of sand with different particle size distributions were used which can be classified as natural, coarse and fine sand. The sieve analysis of the sands was performed in accordance with the ASTM C136 standard test method for the sieve analysis of fine and coarse aggregates. The gradation curves of the sands are presented in Figure 3.2.

To adjust the flowability and viscosity of 3D-printable cement-based mortars, chemical admixtures were also incorporated. Sika Viscocrete Hi-tech 3073 and Sika Viscocrete PC-61 were used as superplasticizers, while Sika Stabilizer 4R-7 was used as a viscosity-modifying agent. The dosage of each chemical admixture was optimized based on the required flow properties and 3D printability of the mixtures.

Figure 3.2: The gradation curve of sands

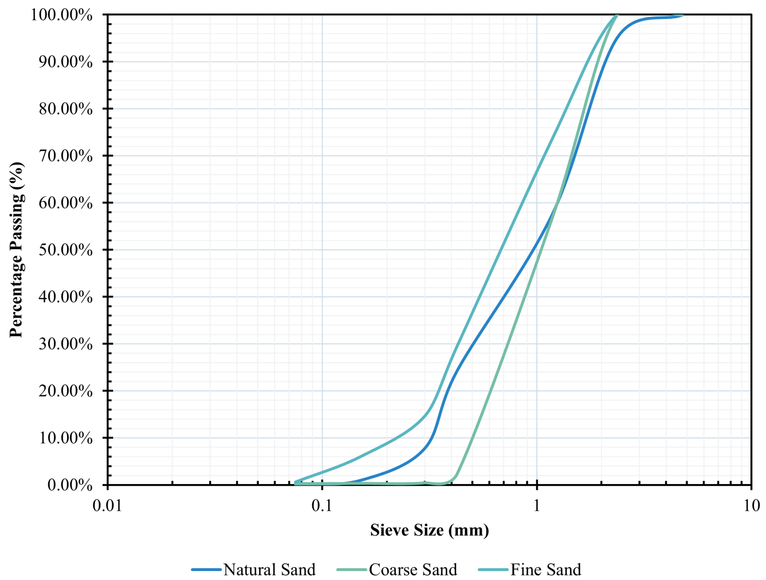

Lastly, Sika Fiber PPM-12, a 12 mm monofilament polypropylene-based fiber was used to evaluate its effect on the mechanical performance of 3D-printed mortars. Both fiber-reinforced and neat cement-based mortars were prepared.

3.2 Mix design and sample preparation

Cement-based mortars were prepared in accordance with ASTM C305-14 Standard Practice for Mechanical Mixing of Hyraulic Cement Pastes and Mortars of Plastic Consistency. The mix proportions of mortars are presented in Table 3.1.

Table 3.1: The mix proportions

	CEM-I	**Fly Ash**	**Recycled Concrete Fine**	**NM**	**Water**	**Coarse Sand**	**Fine Sand**	**Natural sand**	**Sika Viscocrete Hi-tech 3073**	**Sika PC-61**	**Sika Stabilizer 4R-7**	**Fiber**
control	900	-	-	-	324	1000	500	-	5.5	-	1.2	-
control-fiber	900	-	-	-	324	1000	500	-	7.5	-	1.2	1.35
control-FA	720	180	-	-	324	1000	500	-	5.5	-	1.2	-
control-FA-fiber	720	180	-	-	324	1000	500	-	7.5	-	1.2	1.35
NM-FA	711	180	-	9	324	1000	500	-	6	-	-	-
NM-FA-fiber	711	180	-	9	324	1000	500	-	7.2	-	-	1.35
RAP-C	765	-	135	-	360	-	-	1350	-	5.00	0.5	-
RAP-C-fiber	765	-	135	-	360	-	-	1350	-	5.00	0.5	1.35

3.3 Methods

3.3.1 Flowability

The flowability of cement-based mortars was determined in accordance with the American Society for Testing and Materials (ASTM) C1437-07 standard. This test was conducted immediately following the mixing process. Specifically, the flow of the mortar was measured by the spread of fresh mortar pulled out of a cone with a top diameter of 70 mm, a bottom diameter of 100 mm, and a height of 50 mm. After mixing, the conical mold was filled with fresh mortar in two layers. Each layer was tamped 20 times, and the excess material was cleaned off the top of the cone. The fluidity mold was lifted off vertically,and the flow table was immediately dropped 25 times in 15 seconds. After 25 blows, the spread diameter (Figure 3.3) was recorded.

Four measurements were performed for each mix, and the average value and the standard deviation were reported. The flow rate of cement-based mortars were determined according to the following formula Eq.(3.1):

$$\text{Flow Rate } \% = \left(\frac{A}{d_{\text{base}}}\right) \times 100 \tag{3.1}$$

Figure 3.3: The flow table test

3.3.2 3D-printing of cement-based mortars

In the 3D-printing process, a caulking gun was used to extrude cement-based mortar layer by layer, as shown in Figure 3.4. A rectangular nozzle was used to extrude three layers of cement-based mortar. The total height of the three extruded layers was 60 mm.

Figure 3.4: 3D-printing of cement-based mortars

To compare the mechanical behaviour of 3D-printed samples with traditionally cast samples, 4x4x16 cm and 5x5x5 cm molds Figure 3.5 were used to extract samples from 3D-printed layers. The samples exceeded the standard test dimensions. Therefore, after the initial setting time, the dimensions of the 3D-printed samples were gently adjusted.

Figure 3.5: Beam and cube molds to extract samples

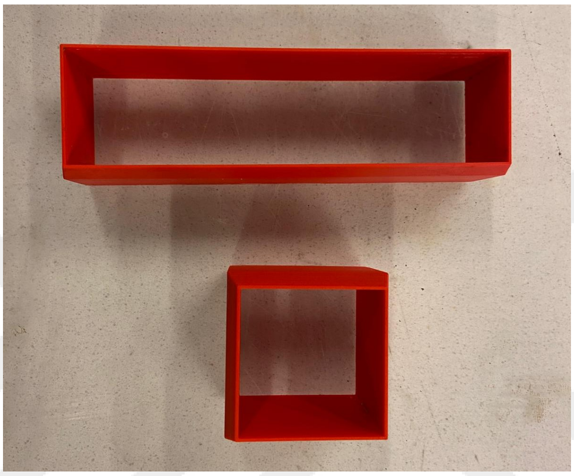

3.3.3 Mechanical properties

The mechanical performance of traditionally cast and 3D printed samples was evaluated in terms of compressive and flexural strength. The test was carried out according to EN 196-1: 2016 (Cement testing methods - Strength determination) and ASTM C109 / C109M-21 (Standard test method for compressive strength of hydraulic cement mortars using 2-in or [50 mm] Cube samples). Mechanical performance was assessed at 7 days and 28 days after casting. A total of six beams with dimensions of 40 mm × 40 mm × 160 mm and six cubes with dimensions of 50 mm × 50 mm × 50 mm were cast. The samples were cured in a climate chamber maintained at 23 ± 1 °C and 50 ± 5% relative humidity.

The flexural strength of the beam specimens was determined using a three-point bending machine with a span distance of 100 mm. The flexural strength was calculated according to the following formula Eq. **(3.2)**

$$F_f = \frac{PL}{bd^2} \tag{3.2}$$

where F_f is the flexural strength of the samples (MPa), P is the maximum applied load of the fracture of the sample and L, b and d are the length of the sample (mm), width (mm) and thickness (mm), respectively.

The fractured portions of the beams resulting from the flexural strength test were subsequently placed into a 40 mm × 40 mm compressive apparatus to determine their compressive strength. Additionally, the 50 mm × 50 mm cube samples were tested to evaluate their compressive strength independently. The compressive strength was calculated according to Eq.(3.2).

$$F_c = \frac{P}{A} \tag{3.3}$$

where F_c is the compressive strength (MPa) of the sample, P is the maximum load applied to the specimen, and A is the area of the loaded surface (mm^2).

3.4 Proposed test procedure for measuring shear strength

The test specimen proposed to measure concrete shear strength is a modified specimen that used by Chandrashekharamurthy et al. [51]. The shear strength of concrete is evaluated by subjecting push-off specimens shown in Figure 3.6 to direct shear loading. The test setup involves specimens with dimensions of 230 mm × 150 mm × 150 mm, which is to be loaded under uniaxial compression using a compression testing machine. Shear strength is calculated as the ratio of the ultimate shear force at failure to the shear area of the push-off specimen along plane B-B.

For the test specimen shown in Figure 3.6, three potential failure modes may occur

Figure 3.6: Proposed push-off test specimen dimensions

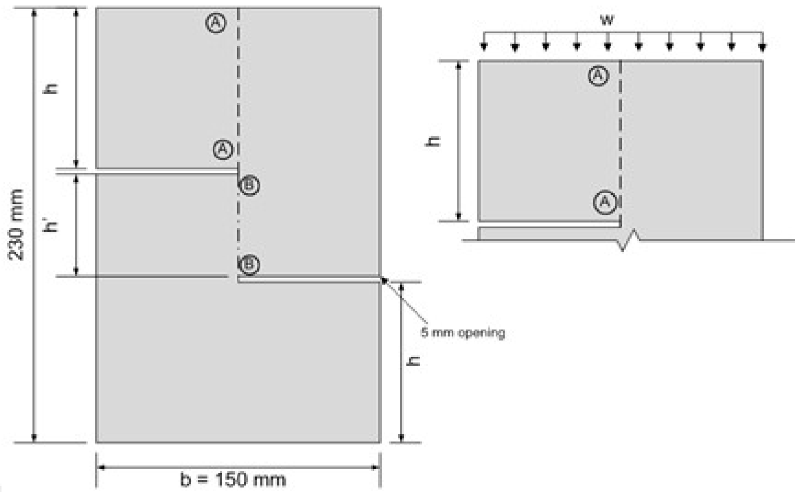

under vertical loading: bending failure along plane A-A, shear failure along plane A-A, and shear failure along plane B-B. The geometry of the specimen is specifically designed to promote shear failure along the predefined shear plane B-B. However, the original specimen dimensions h= 60 mm and h' = 100 mm have been found to be inadequate for ensuring that shear failure occurs along plane B-B prior to shear or bending failure along A-A plane. One potential failure mode is along the A-A plane due to shear force,V_A, acting on shear area, A_A. The shear force and shear stress along the A-A plane are given as a function of specimen loading w, width b, thickness a, and dimensions of the planes h and h'.

$$V_A = w * \frac{b}{2} * a \tag{3.4}$$

$$\tau_A = \frac{V_A}{A_A} = \frac{w * a * \frac{b}{2}}{h * a} = \frac{w * b}{2h} \tag{3.5}$$

Another potential failure mechanism is bending (cracking) failure along A-A plane. The moment and maximum bending stress, which is in tension and potentially can crack the section are given as:

$$M_A = w * \frac{b}{2} * \frac{b}{4} * a = w * \frac{b^2 * a}{8} \tag{3.6}$$

$$\sigma_A = \frac{M_A * \frac{h}{2}}{a * \frac{h^3}{12}} = \frac{6M_A}{a * h^2} = \frac{3w * b^2}{4h^2} \tag{3.7}$$

The desired failure mode is shear failure along B-B plane due to shear force VB along shear area AB, and it is given as:

$$V_B = w * b * a \tag{3.8}$$

$$\tau_B = \frac{V_B}{A_B} = \frac{w * b * a}{h' * a} = \frac{w * b}{h'} \tag{3.9}$$

For an isotropic material under pure shear, the maximum principal tensile stress is equal in magnitude to the shear stress. Assuming that the material shear and tensile strengths are equal, shear failure along B-B plane will govern the failure behavior only if shear stress τ_B acting on that plane is the highest among all stresses on potential failure planes. This condition is checked with the following equations:

For shear along B-B and A-A planes:

$$\tau_B > \tau_A = \frac{w * b}{h'} > \frac{w * b}{2h} = h' < 2h \tag{3.10}$$

For shear along B-B plane and tension along A-A plane:

$$\tau_B > \sigma_A = \frac{w * b}{h'} > \frac{3w * b^2}{4h^2} = h' < \frac{4h^2}{3b} \tag{3.11}$$

To satisfy the conditions listed above, the test specimens with dimensions of 230 mm × 150 mm × 150 mm and b= 150 mm, h =85 mm, and h' =50 mm is recommended to ensure shear failure occur along the desired B-B plane before any other failure occurs.

3.4.1 Numerical Simulation Shear Failure of Test Specimen

The failure mode of the concrete specimen is numerically studied using ABAQUS finite element program [Give reference]. Typical concrete material stress-strain curves are used as shown in Figure 3.7. The concrete compressive strength is taken as 20 MPa with an initial modulus of elasticity of 26000 MPa. The tension strength is assumed to be 1.8 MPa. The modulus of elasticity for the tension is taken same as that for the compression. The specimen is mainly subjected to shear loading; therefore, the compression strength of concrete is assumed to remain at 20 MPa for numerical stability. In the finite element simulation, the concrete specimen is sandwiched between the two rigid loading plates.

Figure 3.7: Concrete stress-strain curves

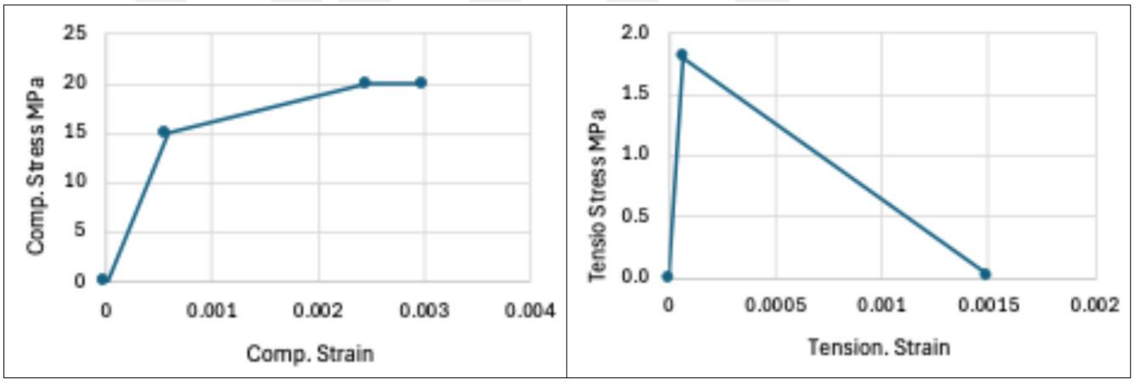

The finite element model developed for the test specimen is shown in Figure 3.8 The developed model is a 3D solid model. The model is partitioned to ensure uniform mesh especially in the location of shear failure. A nominal mesh size 7.5 mm is used for the model. The small mesh size is selected due to two gap openings of 5.0 mm. The solid element C3D8R, which is a three-dimensional, 8-node linear brick element with reduced integration, designed for efficient modeling of solid continuum problems, including concrete structures. Each node has three translational degrees of freedom, allowing for the simulation of complex deformation patterns in concrete under various loading conditions.

The reduced integration scheme, utilizing a single integration point, enhances computational efficiency. The C3D8R element supports Concrete Damaged Plasticity (CDP) material model, which captures the inelastic behavior of concrete including tensile cracking and compressive crushing. Although the element does not model cracks explicitly, damage is represented through stiffness degradation in the material model.

Figure 3.8: Finite element model

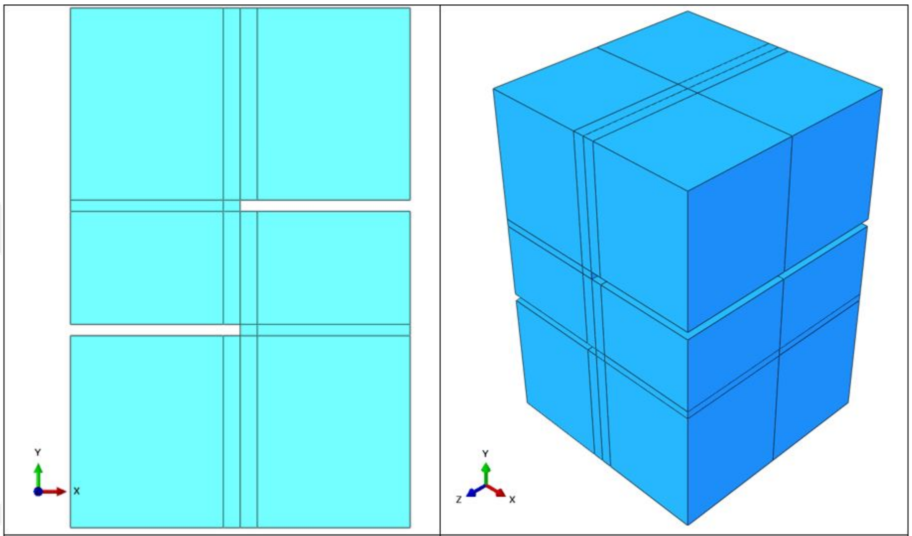

(a) side view | (b) 3D view

The test specimen is to be tested between two plates of testing machine. Therefore, the model is fixed for the displacement at the base surface as shown in Figure 3.9. To allow specimen expansion due to Poison ratio, the base nodes are allowed to displacement in radial direction. In addition, the top surface center node is fixed for lateral displacement for stability. The load is applied as top surface displacement to simulate testing machine plate moving down during testing.

The analysis is performed using Abaqus explicit analysis. Although Abaqus/Explicit is primarily designed for modeling highly dynamic events, it can also be effectively used to solve quasi-static problems, including those under slow loading conditions. To model a static problem using Abaqus/Explicit, the loading must be applied gradually to

Figure 3.9: Finite element mesh

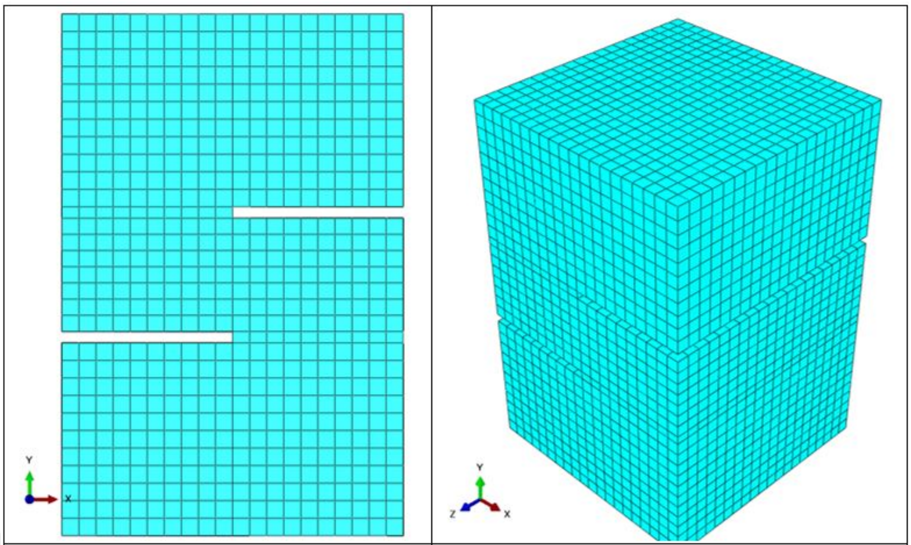

(a) side view	(b) 3D view

ensure that inertial effects remain negligible, thereby approximating a true static response. This approach is particularly suitable for material damage and failure, where convergence difficulties may arise in Abaqus/Standard. To simulate static behavior efficiently, the load is applied slow enough to ensure that dynamic effects are negligible.

Figure 3.10: Loading and boundary conditions

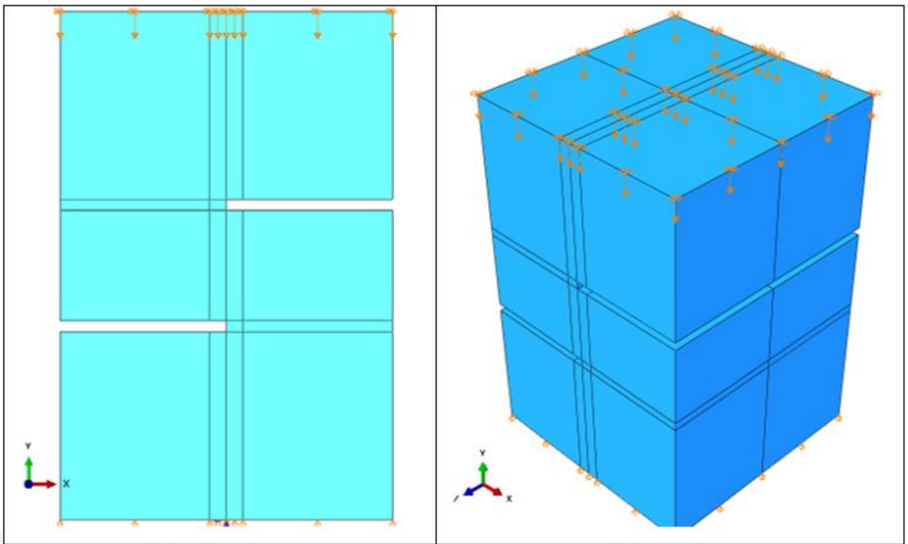

(a) side view

(b) 3D view

3.5 Seismic performance assessment of 3D-printed concrete structures

A numerical model was developed to understand the mechanical response of a 3D-printed wall. The evaluation was done solely using the model without additional experimental tests on a printed wall. Therefore, the material properties were directly incorporated from the data obtained from the literature. The modeled wall has a uniform thickness of 20 mm, an in-plane length of 3000 mm, and a height of 3000 mm, representing a large-scale, unreinforced concrete panel. The material is treated as isotropic, with a compressive strength of 30 MPa and an elastic modulus of 14,400 MPa, values selected to reflect high-performance printable mortar while supporting simplified modeling. No internal reinforcement is included, allowing the analysis to focus solely on the matrix material response under seismic conditions.

The finite element model of a representative 3D-printed wall element is developed using the structural analysis software SAP2000. The geometry and dimensions of this wall are determined to reflect the use of such walls in actual 3-D printed concrete houses.

The wall dimensions are 3 meters in length, 3 meters in height, and 300 mm in depth. The wall also has truss-like segments between the two outer faces, which are intended to enhance the stability and reliability of the wall during the extrusion process. As shown in the finite element model in Figure 3.11, shell elements are used to model all wall parts, including the outer surfaces and the inner truss-like segments. The outer surface shell elements are divided into a mesh size of 30 cm × 30 cm, and inner truss-like elements are connected with the resulting corner nodes of the outer surfaces. The thickness of the shell elements is taken as 2 cm for all surfaces. Each node at the bottom of the wall is pinned to prevent translation in all three directions.

Figure 3.11: Finite element model of the wall element in SAP 2000

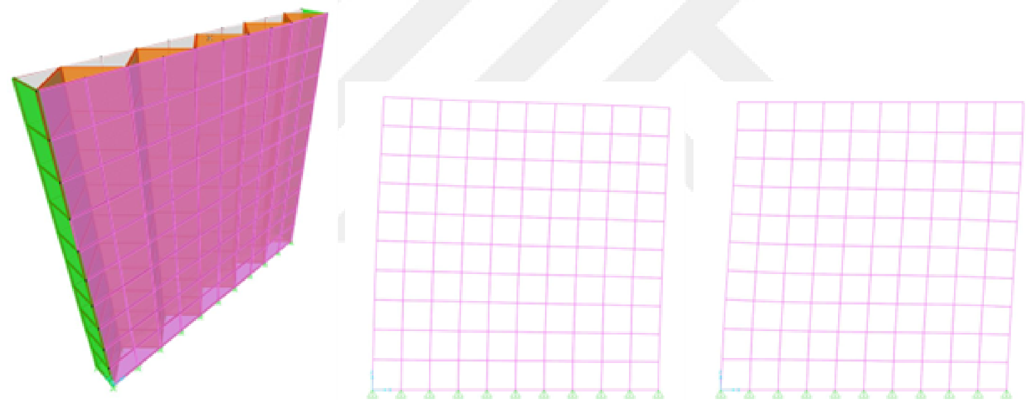

(a) 3D view of the model (b) Deformed shape for PO-1 (c) Deformed shape for PO-1

In the numerical model of the wall, nonlinear material behavior is considered to capture the progression of cracking and redistribution of stresses according to the employed material model for the 3-D printed concrete. Therefore, the outer surfaces and inner truss-like segment of the wall are modeled with layered shell elements, and nonlinear material properties are assigned to these elements to account for the inelastic behavior of concrete. The orthogonal surfaces at the edges are modeled using standard thin-shell elements with linear elastic material properties, as inelastic behavior is not expected on these elements due to the lateral direction of the loading acting along the other wall surfaces. Although anisotropic behavior is typically observed in 3-D printed concrete walls for several reasons, including printing layer orientation, the height of the layer in the structural element, isotropic material behavior is accepted for material definitions in the present study.

In a similar approach as presented in this study, Bayrak (2024) used the finite element analysis software ABAQUS to model a 3D-printed concrete wall specimen using six different material models, aiming to capture the effect of the variation of the material properties along the height of the wall. In that study, experiments were conducted to determine the lateral load capacity of several 3D-printed concrete wall specimens, and the results of the finite element model for one of the specimens were compared with the experimental results. As employed in that study, the stress-strain relationship of the 3D-printed concrete material is generated based on the material properties provided aformentioned and is presented in Figure 3.12. In this material model, stress-strain relationship is considered for compression, while a linear relation is assumed up to the tensile strength and the exponential function is used. However, to have a computational stability stress-strain relationship given for concrete in SAP 2000 is modified and used for the material model assigned to nonlinear shell elements. This material model is also plotted on the same figure in Figure 3.12. A Poisson's ratio of 0.20 is assumed, in line with conventional cementitious materials [52]. The unit weight of the material is taken as 22 kN/m3. No reinforcement is assigned to the model, allowing for a focused evaluation of the unreinforced material.

3.5.1 Pushover Analysis

The main objective in this study is to estimate the in-plane lateral capacity of a full-size 3D-printed concrete wall. For this purpose, a lateral pushover analysis is performed,

Figure 3.12: Material model for the 3D-printed concrete

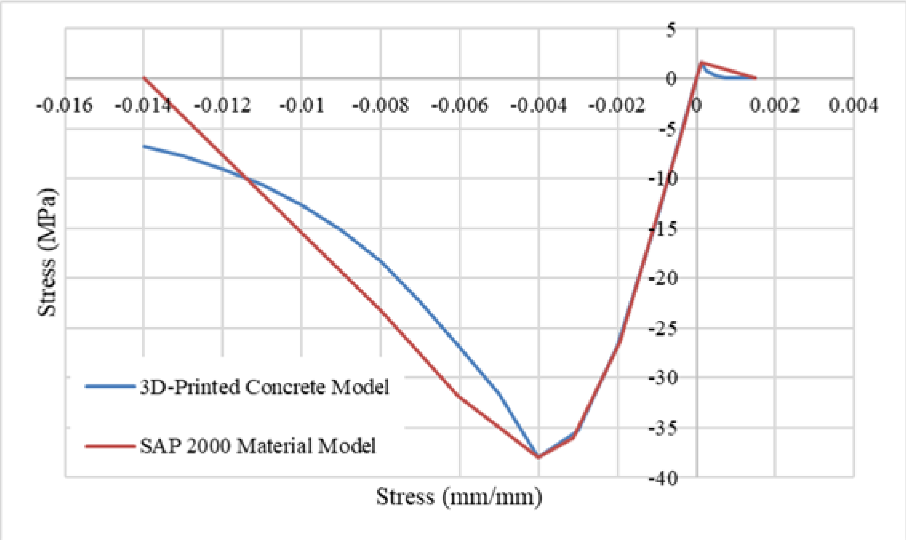

where increasing levels of lateral load is gradually applied on the master node at the top of the wall, and a displacement-controlled loading strategy is used to push the wall until failure. The resulting top displacement is plotted against the total pushing force (or base shear force) to obtain the lateral capacity curve of the wall. The program automatically terminates the analyses when the failure is achieved due to numerical instability, until the targeted top displacement.

Two pushover analyses are conducted in the present study, based on the boundary conditions assigned at the top of the wall. In the first analysis (PO-1), the master node at the top is constrained to have the same translational displacements. In the second analysis (PO-2), this constraint is extended to include rotational degrees of freedom as well. The deformed shapes of the wall for these two analyses are displayed in Figure 3.11.

4. RESULTS AND DISCUSSIONS

4.1 Flowability

In Table 4.1 the flow rates of cement-based mortars are given. Although the flowability of the mortars was suitable for printing, and these mix proportions have previously been tested in terms of 3D-printability, some mortars (RCF and control_FA) exhibited low buildability. Consequently, collapse of the bottom layer was observed when an upper layers was printed. To address this issue, approximately 0.5 g VMA was added to the control_FA mixtures, while for RCF mixtures, the material was allowed to set for a maximum of 30 minutes before printing.

Table 4.1: The flow rate

Sample No	Flow Rate%
control	134%
control-fiber	118%
control-FA	127%
control-FA-fiber	123%
NM-FA	111%
NM-FA-fiber	124%
RAP-C	115%
RAP-C-fiber	116%

4.2 Mechanical properties

Figure 4.1, and Figure 4.2 present 7.day flexural and compressive strengths of traditionally cast and 3D-printed cement-based mortars, respectively. A significant reduction in compressive strength was observed in 3D-printed samples compared to traditionally cast samples. The decrease in compressive strength reached up to 50% when it was 3D-printed. For instance, while the traditionally cast control samples achieved 41 MPa compressive strength, the 3D-printed counterpart exhbited 21 MPa at 7-day. This could be attributed to the bonded interfaces as seen in Figure 4.3 and voids between layers [52]. In contrast, the vibration applied to cast samples minimizes air voids and makes microstructure denser, consequently higher compressive strength.

Figure 4.1: 7. day compressive strength of cement-based mortars according to EN standards

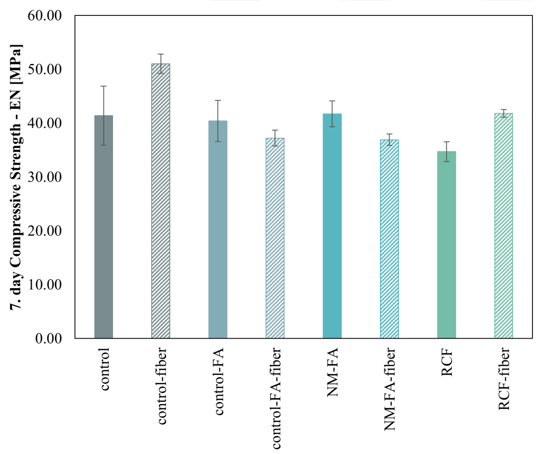

(a) traditionally cast

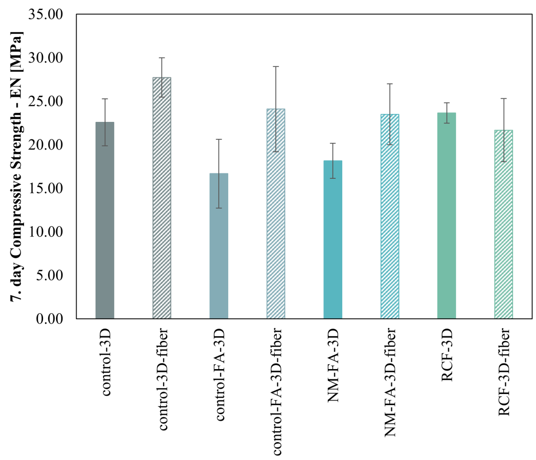

(b) 3D-printed

Figure 4.2: 7. day flexural strength of cement-based mortars

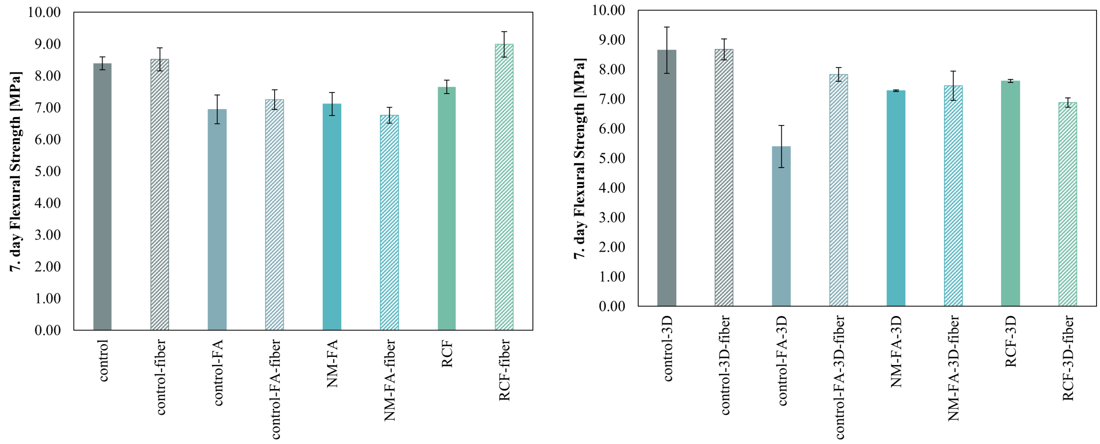

(a) Traditionally cast (b) 3D-printed

When the impact of different mix proportions on the compressive strength were examined, it was seen that FA replacement decreased the compressive strength of cast and 3D-printed samples. However, this reduction was more pronounced in 3D printed samples. The combined effect of the layered structure and slower hydration caused by the pozzolanic effect of FA led to decrease in the compressive strength from 40 MPa to 16 MPa.

Figure 4.3: The bonded interfaces

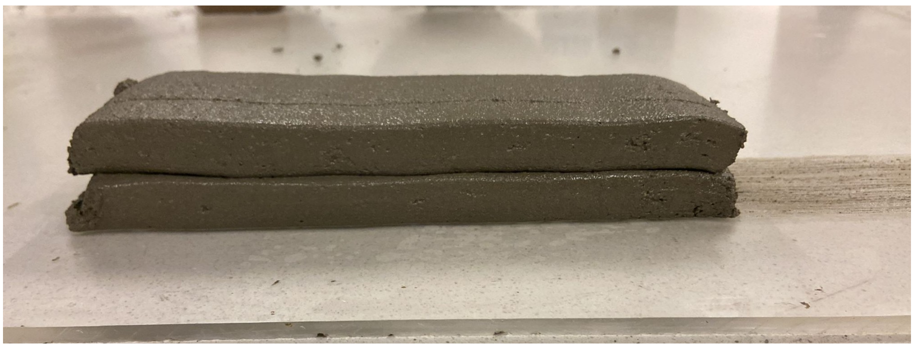

Moreover, NM addition increase compressive strength slightly. Although NM is known as A rheology modifier, the obtained results indicate that it has no significant impact on the compressive strength of 3D-printed samples [5].

Fiber incorporation generally increase the compressive strength of both cast and 3D-printed samples. This enhancement is more pronounced in 3D-printed samples as seen in the compressive strength results. Fibers can fill the gaps between particles due to their deformation ability [53]. Moreover, due to the wall effect of aggregate distribution, the cement paste enriched with fibers tends to settle in the interfacial zones, strengthening the integrity of these weak regions [54]. This impact is critical for 3D-printed samples, where interlayer bonding is a key factor in the mechanical behaviour. In addition, fibers improve the buildability of printed samples, resulting in decreased deformation after extrusion. Consequently, the homogenity of the layers from edge to center is enhanced [53].

The 3D-printed samples and the traditionally cast samples exhibited similar flexural strength. In particular, the mixtures containing FA and fibers showed the lowest flexural strength. This could be attributed to the slower hydration caused by the pozzolanic effect of fly ash. In addition, the incorporation of fiber reduced the flowablity of mortar which makes placement and printing more diffucult. Therefore, entrapped air during placement and tearing and cracking during printing may occur.

4.3 Numerical analysis of 3D-printed wall

4.3.1 Lateral capacity of the wall

Figure 4.4 shows the load-displacement curve of the wall resulting from the two pushover analyses, PO-1 and PO-2. The pushover analysis PO-1 is terminated when the target displacement of 20 mm is reached, while the analysis PO-2 automatically stops at around 15 mm before the target displacement when the wall no longer carries loading. The resulting pushover curve from the analysis PO-2 is assessed to be more realistic and compatible with the lateral behavior as would occur under a seismic loading scenario. A lateral force capacity of 1537 kN is obtained from the pushover curve resulting from PO-2.

Figure 4.4: Pushover curves

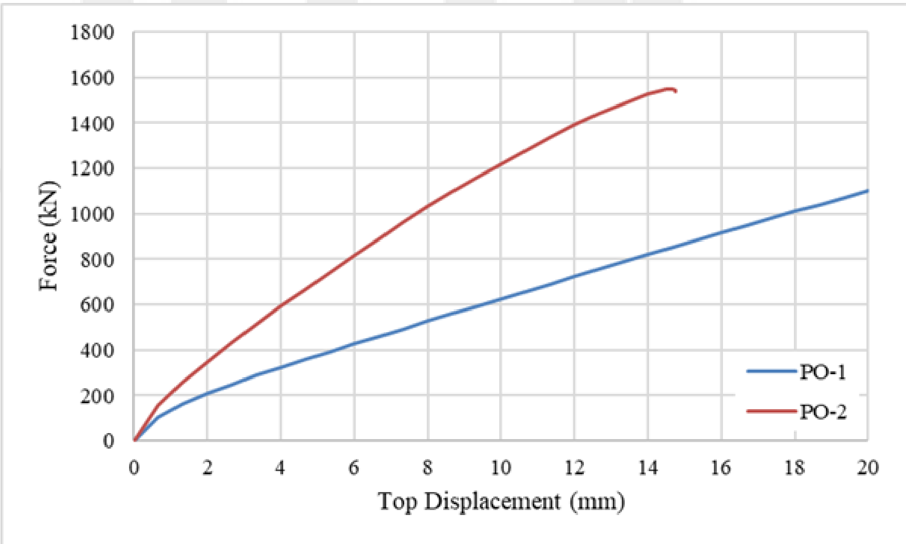

4.3.2 Progression of crack formation

Although no physical crack observation is conducted, crack formation is predicted based on tensile strain concentration and stiffness reduction observed in the analysis outputs Figure 4.5. This approach supports the identification of likely failure zones and the overall lateral resistance capacity of the wall under simulated seismic action.

Figure 4.5: Principle tensile stress on the outer face of the wall

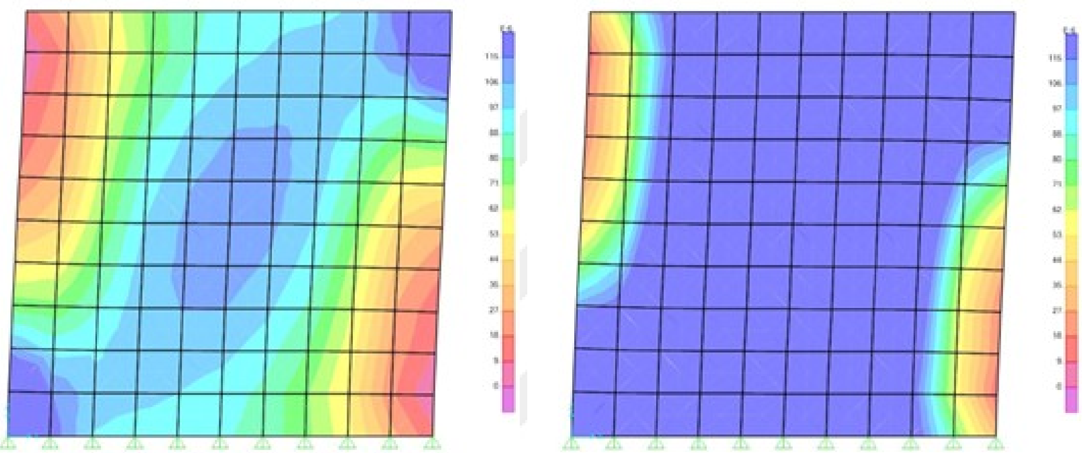

(a) Step 1 (F = 160 kN)

(b) Step 2 (F = 258 kN)

The modeling approach draws conceptually from Bayrak's (2023) work, which employed ABAQUS and a Continuum Damage Plasticity Model (CDPM) to simulate the cyclic behavior of unreinforced 3D-printed concrete walls. The onset of damage and failure was evaluated based on critical tensile strains and overall lateral drift beyond acceptable limits Figure 4.6.

Figure 4.6: Formation of the first crack

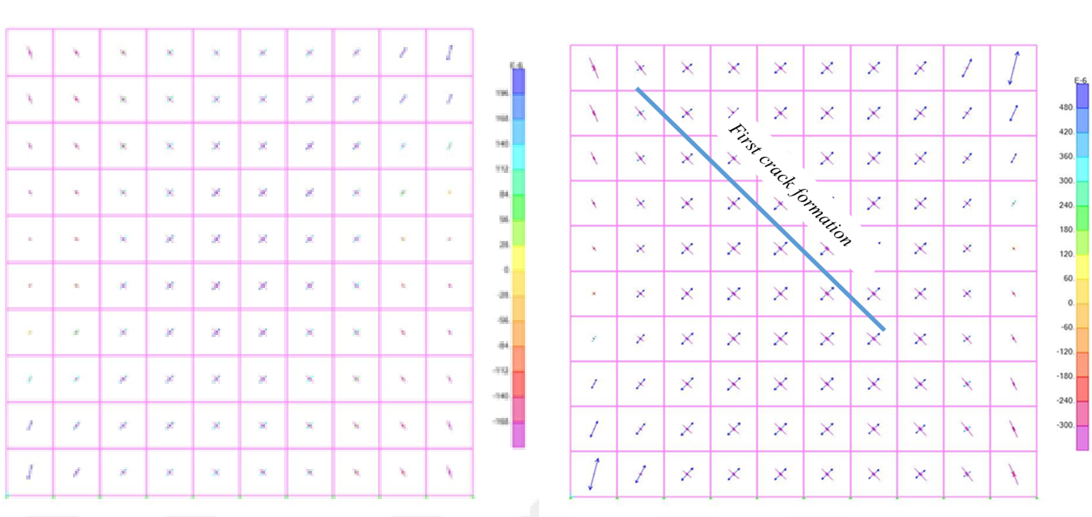

(a) Step 1 (F = 160 kN) (b) Step 2 (F = 258 kN)

4.3.3 Numerical Simulation Shear Failure of Test Specimen

Figure 4.7, Figure 4.8 and Figure 4.9 show the principal maximum strain contours of the specimen under small, medium, and large loading levels, respectively, up to failure. Only strain contours exceeding the concrete cracking strain threshold of 7×10 are displayed. The results indicate that significant tensile strains develop along the intended shear plane, confirming the expected failure mechanism. As the applied load increases, these tensile strains intensify along the shear plane. Figure 4.8 and Figure 4.9 further reveal that the crack path deviates slightly from the vertical, exhibiting a minor inclination. However, this deviation is considered negligible given the nominal mesh size of 7.5 mm. Overall, the strain contour results confirm that cracking will occur as intended, validating the effectiveness of the setup in capturing shear strength along the designated failure plane.

Figure 4.7: Maximum principal strain contours at small loads for strain larger than cracking strain (7E-5)

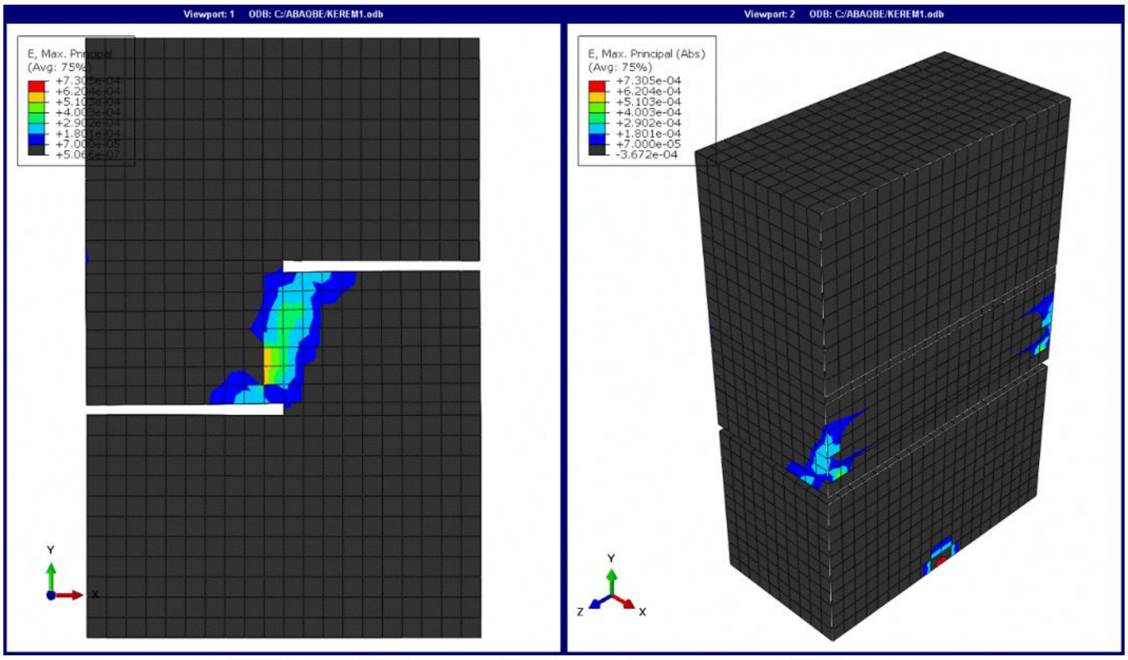

Figure 4.8: Maximum principal strain contours at medium loads for strain larger than cracking strain (7E-5)

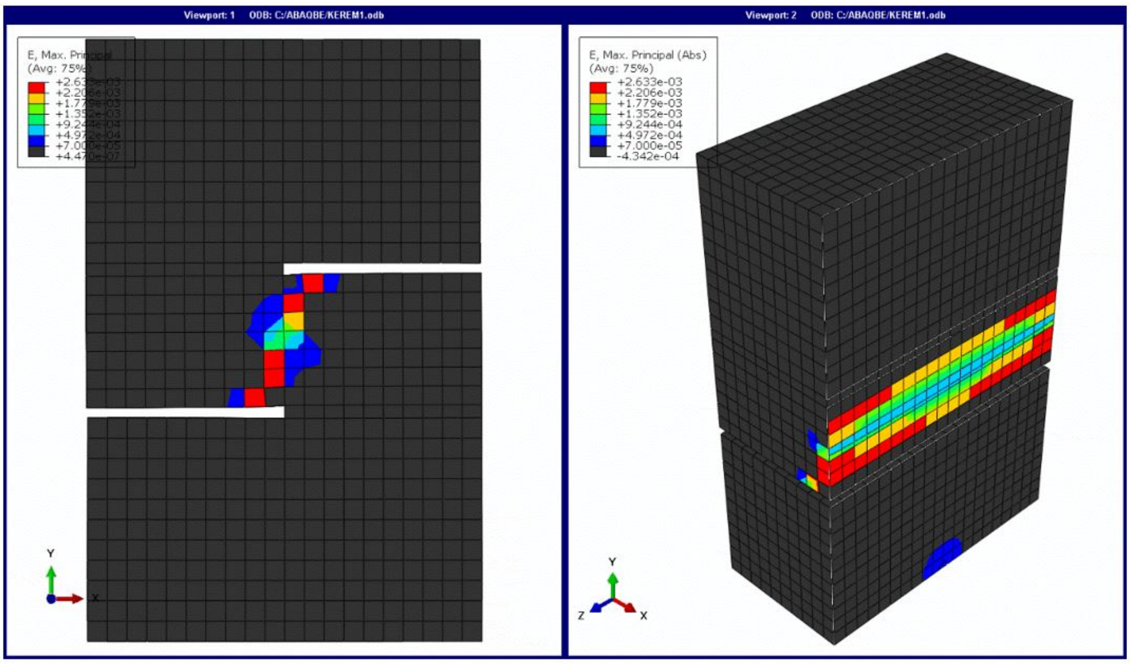

Figure 4.9: Maximum principal strain contours at large loads for strain larger than cracking strain (7E-5)

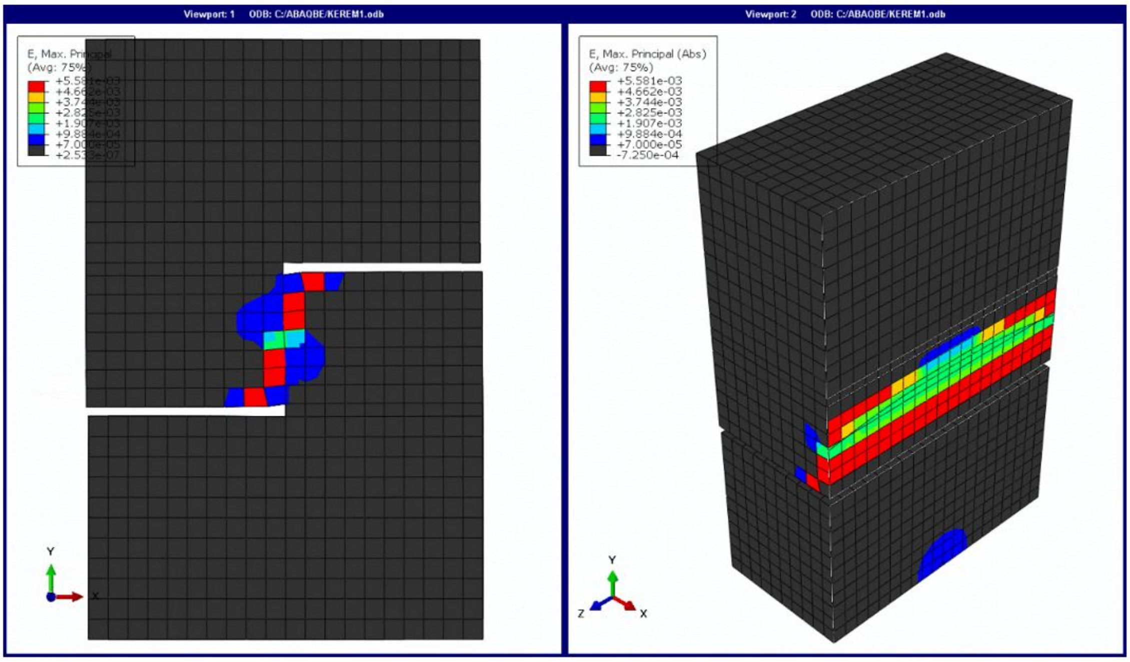

5. CONCLUSIONS

In this study, the mechanical behaviour of 3D-printed and traditionally cast cement-based mortars was compared to evaluate how 3D printing impacts the mechanical performance of the material. Moreover, the seismic performance of an unreinforced, cement-based 3D-printed wall element was assessed through numerical analysis. The outcomes of the study can be summarized as follows:

- While 3D printing does not lead to a significant reduction in the flexural strength of mortars, a notable decrease in the compressive strength of 3D-printed samples was observed compared to traditionally cast samples.
- Using consistent mechanical properties and large-scale geometry, the model provides insight into the structural behaviour of 3D-printed concrete under monotonic lateral displacement. Although the wall is not physically printed or tested, the strain distribution and stress concentrations observed in the simulation enable the prediction of likely crack initiation zones and potential failure modes. These results highlight the vulnerability of unreinforced printed walls to in-plane seismic forces and reinforce the importance of considering interfacial behaviour, material quality, and geometric scaling in future structural assessments of 3D-printed systems.

5.1 Limitations

- The 3D-printing process in this study was conducted using a caulking gun which is operator-dependent. Moreover the molding stage of 3D-printed samples cause damage to the samples. Therefore, the compressive strength test results of 3D-printed mortar samples exhibited a higher standard deviation compared to traditionally cast samples.

5.2 Future Works

- In future studies, the proposed test procedure to determine shear strength should be first applied to both cast and 3D-printed samples.
- To better observe the impact of 3D-printing on the mechanical behaviour of cement-based mortar, advanced 3D-printing systems will be utilized.
- Sampling of 3D-printed mortars will be conducted at different times such as immediately after 3D-printing and after final setting time to minimize and evaluate the effect of sampling time on mechanical behaviour.
- The findings support the development of performance-based evaluation methods for 3D-printed concrete walls and underline the need for further experimental validation and code development to guide their safe application in structural engineering.

REFERENCES

[1] D. Asprone, C. Menna, F. P. Bos, T. A. Salet, J. Mata-Falcón, and W. Kaufmann, "Rethinking reinforcement for digital fabrication with concrete," *Cement and Concrete Research*, vol. 112, pp. 111–121, 2018.

[2] D. Lowke, E. Dini, A. Perrot, D. Weger, C. Gehlen, and B. Dillenburger, "Particle-bed 3d printing in concrete construction–possibilities and challenges," *Cement and concrete research*, vol. 112, pp. 50–65, 2018.

[3] S. Lim, R. A. Buswell, T. T. Le, S. A. Austin, A. G. Gibb, and T. Thorpe, "Developments in construction-scale additive manufacturing processes," *Automation in construction*, vol. 21, pp. 262–268, 2012.

[4] S. S. Benam, I. Sandalci, B. Kara, and O. Bebek, "Improving the 3d printability of high-volume fly ash mixtures through addition of mineral," in *Proceedings of the RILEM Spring Convention and Conference 2024: Volume 2*, vol. 56, p. 265, Springer Nature, 2024.

[5] E. M. Aydin, B. Kara, Z. B. Bundur, N. Ozyurt, O. Bebek, and M. A. Gulgun, "A comparative evaluation of sepiolite and nano-montmorillonite on the rheology of cementitious materials for 3d printing," *Construction and Building Materials*, vol. 350, p. 128935, 2022.

[6] A. Nikravan, T. Aydin, N. Ozyurt, and Z. Basaran Bundur, "Enhancing the performance of 3d-printed fiber-reinforced mortar: synergistic effects of clays and bacterial cells as viscosity modifying agents," *Journal of Sustainable Cement-Based Materials*, vol. 14, no. 3, pp. 506–520, 2025.

[7] A. Kazemian, X. Yuan, R. Meier, and B. Khoshnevis, "Performance-based testing of portland cement concrete for construction-scale 3d printing," in *3D concrete printing technology*, pp. 13–35, Elsevier, 2019.

[8] Y. Weng, M. Li, S. Ruan, T. N. Wong, M. J. Tan, K. L. O. Yeong, and S. Qian, "Comparative economic, environmental and productivity assessment of a concrete bathroom unit fabricated through 3d printing and a precast approach," *Journal of Cleaner Production*, vol. 261, p. 121245, 2020.

[9] V. N. Nerella, M. Krause, and V. Mechtcherine, "Direct printing test for buildability of 3d-printable concrete considering economic viability," *Automation in Construction*, vol. 109, p. 102986, 2020.

[10] J. G. Sanjayan and B. Nematollahi, "3d concrete printing for construction applications," *3D concrete printing technology*, vol. 1, pp. 1–11, 2019.

[11] D. Liu, Z. Zhang, X. Zhang, and Z. Chen, “3d printing concrete structures: State of the art, challenges, and opportunities,” *Construction and Building Materials*, vol. 405, p. 133364, 2023.

[12] O. Ahi, Ö. Ertunç, Z. B. Bundur, and Ö. Bebek, “Automated flow rate control of extrusion for 3d concrete printing incorporating rheological parameters,” *Automation in Construction*, vol. 160, p. 105319, 2024.

[13] S. Paritala, K. K. Singaram, I. Bathina, M. A. Khan, and S. K. R. Jyosyula, “Rheology and pumpability of mix suitable for extrusion-based concrete 3d printing–a review,” *Construction and Building Materials*, vol. 402, p. 132962, 2023.

[14] D. Marchon, S. Kawashima, H. Bessaies-Bey, S. Mantellato, and S. Ng, “Hydration and rheology control of concrete for digital fabrication: Potential admixtures and cement chemistry,” *Cement and Concrete Research*, vol. 112, pp. 96–110, 2018.

[15] B. Panda, S. Ruan, C. Unluer, and M. J. Tan, “Improving the 3d printability of high volume fly ash mixtures via the use of nano attapulgite clay,” *Composites Part B: Engineering*, vol. 165, pp. 75–83, 2019.

[16] E. Najafi and R. Khanbilvardi, “Evaluating global crop distribution in the 21st century to maximize food production,” in *AGU Fall Meeting Abstracts*, vol. 2019, pp. B31F–2440, 2019.

[17] C. R. Gagg, “Cement and concrete as an engineering material: An historic appraisal and case study analysis,” *Engineering Failure Analysis*, vol. 40, pp. 114–140, 2014.

[18] P. J. Monteiro, S. A. Miller, and A. Horvath, “Towards sustainable concrete,” *Nature materials*, vol. 16, no. 7, pp. 698–699, 2017.

[19] U. Environment, K. L. Scrivener, V. M. John, and E. M. Gartner, “Eco-efficient cements: Potential economically viable solutions for a low-co2 cement-based materials industry,” *Cement and concrete Research*, vol. 114, pp. 2–26, 2018.

[20] M. K. Mohan, A. Rahul, G. De Schutter, and K. Van Tittelboom, “Extrusion-based concrete 3d printing from a material perspective: A state-of-the-art review,” *Cement and Concrete Composites*, vol. 115, p. 103855, 2021.

[21] S. Mindess, “Sustainability of concrete,” in *Developments in the Formulation and Reinforcement of Concrete*, pp. 3–17, Elsevier, 2019.

[22] X. Guo, J. Yang, and G. Xiong, “Influence of supplementary cementitious materials on rheological properties of 3d printed fly ash based geopolymer,” *Cement and Concrete Composites*, vol. 114, p. 103820, 2020.

[23] Y. Han, Z. Yang, T. Ding, and J. Xiao, “Environmental and economic assessment on 3d printed buildings with recycled concrete,” *Journal of Cleaner Production*, vol. 278, p. 123884, 2021.

[24] N. B. Shahid, R. Mutsuddy, and S. R. Islam, “Synergistic impact of supplementary cementitious materials (silica fume and fly ash) and nylon fiber on properties of recycled brick aggregate concrete,” *Case Studies in Construction Materials*, vol. 22, p. e04484, 2025.

[25] Y. Guo, Q. Lu, G. Du, and J. Zhang, “Mechanical properties of concrete with low-content rubber particles co-reinforced by silica fume and steel fiber under freeze-thaw cycles,” *Construction and Building Materials*, vol. 490, p. 142515, 2025.

[26] S. D. C. Gomes, Q. D. Nguyen, W. Li, and A. Castel, “Shrinkage and carbonation of alkali-activated calcined clay-ground granulated blast furnace slag (ggbfs) concrete,” *Cement and Concrete Research*, vol. 194, p. 107899, 2025.

[27] J. Fan and B. Zhang, “Study on the effect of modified zeolite powder on curing mechanism of concrete,” *Construction and Building Materials*, vol. 483, p. 141830, 2025.

[28] K.-H. Ler, C.-K. Ma, C.-L. Chin, I. S. Ibrahim, K. H. Padil, M. A. I. Ab Ghafar, and A. A. Lenya, “Porosity and durability tests on 3d printing concrete: A review,” *Construction and Building Materials*, vol. 446, p. 137973, 2024.

[29] H. Els, G. van Zijl, and W. de Villiers, “A review of shrinkage and restrained shrinkage cracking in 3d concrete printing,” *Journal of Building Engineering*, p. 113233, 2025.

[30] R. A. Buswell, W. L. De Silva, S. Z. Jones, and J. Dirrenberger, “3d printing using concrete extrusion: A roadmap for research,” *Cement and concrete research*, vol. 112, pp. 37–49, 2018.

[31] S. C. Paul, G. P. Van Zijl, M. J. Tan, and I. Gibson, “A review of 3d concrete printing systems and materials properties: Current status and future research prospects,” *Rapid Prototyping Journal*, vol. 24, no. 4, pp. 784–798, 2018.

[32] S. K. Kaliyavaradhan, P. Ambily, P. R. Prem, and S. B. Ghodke, “Test methods for 3d printable concrete,” *Automation in Construction*, vol. 142, p. 104529, 2022.

[33] E. Kaya, B. Ciza, Ç. Yalçınkaya, B. Felekoğlu, H. Yazıcı, and O. Çopuroğlu, “A comparative study on the effectiveness of fly ash and blast furnace slag as partial cement substitution in 3d printable concrete,” *Journal of Building Engineering*, p. 112841, 2025.

[34] M. Chen, B. Liu, L. Li, L. Cao, Y. Huang, S. Wang, P. Zhao, L. Lu, and X. Cheng, “Rheological parameters, thixotropy and creep of 3d-printed calcium sulfoaluminate cement composites modified by bentonite,” *Composites Part B: Engineering*, vol. 186, p. 107821, 2020.

[35] P. Jin, M. Hasany, M. Kohestanian, and M. Mehrali, "Micro/nano additives in 3d printing concrete," *Cement and Concrete Composites*, vol. 155, p. 105799, 2025.

[36] J.-J. Zeng, X. Hu, H.-Q. Sun, Y. Liu, W.-J. Chen, and Y. Zhuge, "Triaxial compressive behavior of 3d printed pe fiber-reinforced ultra-high performance concrete," *Cement and Concrete Composites*, vol. 155, p. 105816, 2025.

[37] C. Liu, M. Zou, X. Chen, Y. Deng, L. Zhang, X. Luo, and L. Liu, "Feasibility study of 3d-printed rubberized concrete as a permanent formwork: mechanical properties, interlayer interface and durability," *Journal of Building Engineering*, vol. 106, p. 112544, 2025.

[38] J. Cai, J. Wang, Q. Zhang, C. Du, M. Meloni, and J. Feng, "State-of-the-art of mechanical properties of 3d printed concrete," *Case Studies in Construction Materials*, vol. 21, p. e03847, 2024.

[39] H. K. Chandrashekharamurthy, W. P. Prema Kumar, and M. T. Prathap Kumar, "Shear strength, compressive strength and workability characteristics of concretes reinforced with steel fibres," *International Journal of Engineering Research & Technology (IJERT)*, vol. 8, pp. 10–??, June 2019. Paper ID IJERTV8IS060035.

[40] J. Hofbeck, I. Ibrahim, and A. H. Mattock, "Shear transfer in reinforced concrete," in *Journal Proceedings*, vol. 66, pp. 119–128, 1969.

[41] Z. P. Bažant, "Size effect in blunt fracture: concrete, rock, metal," *Journal of engineering mechanics*, vol. 110, no. 4, pp. 518–535, 1984.

[42] A. M. Sonnenberg, R. Al-Mahaidi, and G. Taplin, "Behaviour of concrete under shear and normal stresses," *Magazine of concrete research*, vol. 55, no. 4, pp. 367–372, 2003.

[43] Y. Hamadi and P. Regan, "Behaviour in shear of beams with flexural cracks," *Magazine of Concrete Research*, vol. 32, no. 111, pp. 67–78, 1980.

[44] M. Mansur, T. Vinayagam, and K.-H. Tan, "Shear transfer across a crack in reinforced high-strength concrete," *Journal of Materials in Civil Engineering*, vol. 20, no. 4, pp. 294–302, 2008.

[45] J. Xiao, H. Xie, and Z. Yang, "Shear transfer across a crack in recycled aggregate concrete," *Cement and Concrete Research*, vol. 42, no. 5, pp. 700–709, 2012.

[46] M. Valle and O. Buyukozturk, "Behavior of fiber reinforced high-strength concrete under direct shear," *Materials Journal*, vol. 90, no. 2, pp. 122–133, 1993.

[47] C. Li, Z. Feng, L. Ke, R. Pan, and J. Nie, "Experimental study on shear performance of cast-in-place ultra-high performance concrete structures," *Materials*, vol. 12, no. 19, p. 3254, 2019.

[48] Y. Shi, Y. Lu, and J. Cui, "Experimental study on dynamic mechanical properties of concrete under direct shear loading," *Cement and Concrete Composites*, vol. 142, p. 105150, 2023.

[49] M. Zajac, J. Skocek, M. Ben Haha, and J. Deja, "Co2 mineralization methods in cement and concrete industry," *Energies*, vol. 15, no. 10, 2022.

[50] Q. Wang, Z. Xiong, J. He, M. Lai, and J. Ho, "Effective solution for improving rheological properties of cement paste containing zeolite," *Construction and Building Materials*, vol. 351, p. 128780, 2022.

[51] R. Naserian *et al.*, "Shear strength, compressive strength and workability characteristics of concretes reinforced with steel fibres," *International Journal of Engineering Research & Technology (IJERT)*, vol. 8, p. –?, June 2019.

[52] Z. Pan, D. Si, J. Tao, and J. Xiao, "Compressive behavior of 3d printed concrete with different printing paths and concrete ages," *Case Studies in Construction Materials*, vol. 18, p. e01949, 2023.

[53] Y. Zhang, Y. Zhu, Q. Ren, B. He, Z. Jiang, K. Van Tittelboom, and G. De Schutter, "Comparison of printability and mechanical properties of rigid and flexible fiber-reinforced 3d printed cement-based materials," *Construction and Building Materials*, vol. 400, p. 132750, 2023.

[54] K. H. Khayat, W. Meng, K. Vallurupalli, and L. Teng, "Rheological properties of ultra-high-performance concrete — an overview," *Cement and Concrete Research*, vol. 124, p. 105828, 2019.